Final Technical Report
DOE grant DE-FG02-99ER15003 "Model Catalysis by Size-Selected Cluster Deposition"
PI: Scott Anderson, Chemistry Department, University of Utah, 315 S. 1400 E. Rm. 2020, Salt Lake City, UT 84112. 801-585-7289, FAX: 801-581-8433, anderson@chem.utah.edu

I. Introduction

This grant started in 1999, and progress reports have been filed annually, with more detailed annual reports filed tri-annually. This report will focus on the results obtained in the past 5 years.

Goals: Supported catalysts are involved in ~20% of the US GDP, and improved understanding of the factors that control catalyst and electrocatalyst activity would be valuable in understanding catalytic mechanisms and designing improved new catalysts. This project has taken advantage of unique instrumentation, developed partially with DOE support, that allows preparation of model catalysts with size-selected metal clusters deposited on well-characterized planar supports in ultra-high vacuum (UHV). These catalysts can then be studied *in situ* without air exposure, allowing detailed studies of their physical and chemical properties, including catalysis under both gas-surface and aqueous electrochemical conditions. The work, therefore, has focused on determining the effects of catalytic site size on activity and product branching. In addition, we have searched for size-dependent correlations between fundamental cluster physical properties and activity or selectivity for the catalytic reactions. When such correlations are found, they reveal what factors control activity and selectivity.

II. Experimental Approach

A. Cluster deposition and UHV surface science capabilities:

The experiments were performed using the instrument shown in Fig. 1, consisting of a mass-selected ion deposition beamline (top of figure), connected to an ultrahigh vacuum (UHV) deposition/analysis chamber (bottom; pressure ~10^{-10} Torr). Operating procedures are described in several papers.[1-7] Briefly, clusters are generated using a laser vaporization source operating at 30 Hz, and a magnetron sputtering/gas aggregation source is also available. Cluster ions are collected by a series of quadrupole ion guides, and passed through differential pumping stages to separate the cluster ions from the large flow of helium gas in the source. The beamline includes a bend to allow co-axial injection of the vaporization laser, and prevent neutrals exiting the source from reaching the sample. The beam is passed through a quadrupole mass filter to select the cluster size and composition.

A final quadrupole guides the mass-selected clusters into the main UHV chamber, where they are deposited through a 2 mm diameter mask onto a planar substrate, positioned ~ 200 μm behind the mask. Deposition current is integrated to determine the cluster coverage. To allow study of size effects, samples are prepared with identical coverage of metal, deposited in the form of different size clusters. In most of the example results given below, the metal coverage was equivalent to 0.1 of a close-packed monolayer, with samples differing only in what size cluster was deposited. Deposition has typically been done at 1 eV/atom energy, based on studies where sample properties were found to change only for energy above 3 - 5 eV/atom.[8, 9]

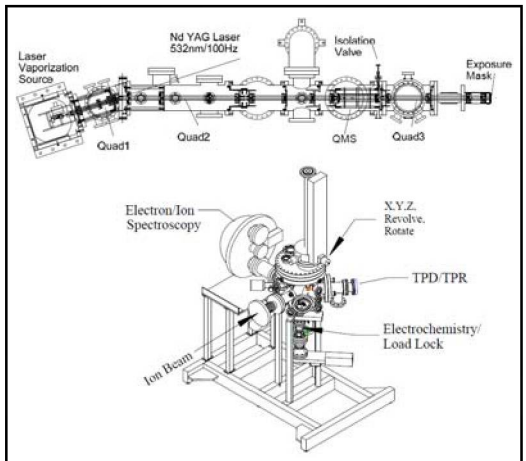

Fig. 1. Schematic of instrument. The beamline (top) inserts into the port labeled "Ion Beam" in lower portion of the figure.

Deposition supports have typically been either oxide single crystals or thin films for UHV studies, and for the electrochemistry studies we used glassy carbon wafers or indium-tin oxide (ITO) thin films. The support is mounted to the bottom of a small cryostat, with provisions for both resistive and e-beam heating for temperature control from ~120 K to >2200 K. The main UHV chamber also has facilities for support cleaning/annealing and growth of epitaxial films, for *in situ* characterization by x-ray and UV

photoelectron spectroscopy (XPS, UPS), low energy ion scattering spectroscopy (ISS), and for mass spectrometric probing of adsorbate binding and reactions under gas-surface conditions. XPS probes the top several nanometers of the sample, and provides insight into the electronic environment of the metal clusters, and how it is affected by binding of adsorbates. UPS gives corresponding information about valence energy levels. ISS is sensitive to the identity and relative abundance of each type of atom in the top-most layer of the sample. In combination with XPS, ISS provides insight into cluster morphology, and is also useful for monitoring sintering of the clusters. The mass spectrometer is differentially pumped, and has both pulsed and continuous gas inlets aimed at the sample. Temperature-programmed desorption (TPD) provides insight into the density and energetics of adsorbate binding sites, and in conjunction with ISS (temperature-dependent ISS), gives information about adsorbate binding sites.[1, 5] Analogous temperature-programmed reaction (TPR) studies probe the activity, product branching, and energetics for reactions. Experiments where the sample is exposed to continuous or millisecond pulsed flows of reactants at fixed or ramped surface temperature, allow measurement of reactions as a function of reactant flux, and under conditions where one or more reactant does not stick.[10-12]

B. *In situ* electrochemistry:

The bottom of the main UHV chamber has a triple differentially pumped seal assembly, to which we can attach any one of several antechambers, pumped by a small turbo and TSP, with base pressure in the mid-10^{-10} Torr range. When the sample is in the antechamber, it is isolated, allowing high pressure operations like film growth or electrochemistry with no effect on the main chamber vacuum. To enable electrochemical study of size-selected electrodes to be performed with minimal perturbation from adventitious adsorbates, we developed, with DOE support, an *in situ* UHV-compatible electrochemical cell (Fig. 2) which is housed in the antechamber shown in Fig. 3.[13, 14] One compartment of the cell contains a Pt mesh counter electrode, another contains an Ag/AgCl reference electrode, and the third is open at one end, allowing it to be sealed via an o-ring to the working electrode, surrounding the 2 mm spot of deposited clusters.

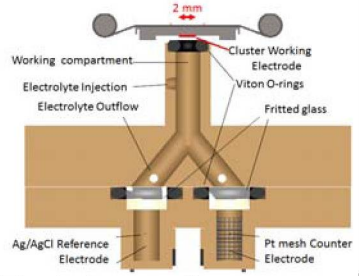

Fig. 2. *In situ* cell

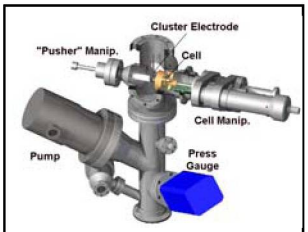

Fig. 3. New electro-chemistry antechamber

Using Pt clusters as an example, a typical electrochemistry protocol begins with loading a fresh electrode onto the sample holder in the antechamber, and baking the antechamber at 400 K and 10^{-8} Torr overnight. The electrode is then pulled into the main chamber and cleaned by sputtering and/or annealing in UHV as appropriate for the electrode type. XPS is used to check for contamination, and then a particular size Pt_n is deposited in a 2 mm spot on the electrode, with deposition current used to control the Pt_n coverage precisely. XPS is then used to characterize the as-deposited Pt_n electrode. (UPS, ISS, and gas adsorption experiments can be done as well, but those are done on separate samples). The electrode is then lowered into the antechamber, which is pressurized to just above 1 atm with UHP argon. The electrochemical cell is sealed to the electrode surrounding the cluster spot, and then electrolytes are pumped into the cell, and a potentiostat is used study electrocatalytic activity, typically by measuring cyclic voltammograms (CVs). After completion of electrochemistry, the antechamber and cell are cleaned, and a new electrode is loaded to prepare for the next day's work.

III. Experiments reported in the last five years of the grant (complete list below):

All papers listed in the text acknowledged DOE support from this grant. Papers cited by superscript numbers refer to the bibliography section, and may or may not have been supported by this grant.

1. Surface Science Experiments:

Characterizing Reactivity: In 2009 we published a paper *(Surf. Sci. 603 (2009) 2764-77)* in which we showed that the oxygen affinity of Pd_n clusters deposited on alumina films grown on NiAl(110) is anticorrelated with the Pd 3d binding energy (BE) measured by XPS. Unfortunately, because the alumina film that grows on NiAl(110) is too thin to act as an O atom diffusion barrier, it was not possible study oxidation chemistry catalyzed by the Pd clusters.

To allow such studies, we switched to studying Pd clusters deposited on single crystal TiO_2(110),

and in a paper the same year *(Science 326, (2009) 826)* we reported the first observation of a strong anti-correlation between electron BEs and activity for a chemical reaction - CO oxidation catalyzed by $Pd_n/TiO_2(110)$. Fig. 4 compares activity vs. deposited cluster size (left axis), with shifts in the Pd 3d BE (right axis – inverted scale), relative to the bulk Pd BE, with an estimated correction for final state charging. This result basically says that catalysts in which the Pd 3d BE is particularly low are particularly active. As shown below we have now seen similar anti-correlations between metal BEs and activity for oxidation catalysis in several other systems, including two involving electrocatalysis.

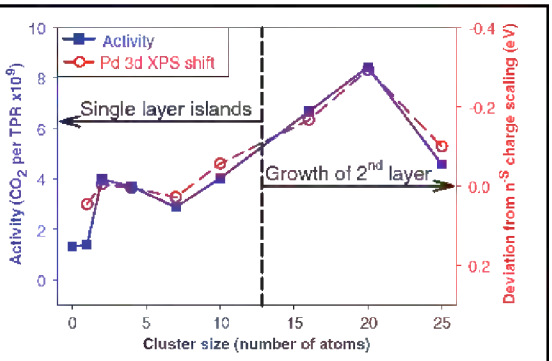

Fig. 4. Activity for CO_2 production as a function of cluster size (left axis) under conditions of O_2 exposure at 400 K, and CO exposure at 180 K. Pd 3d BEs, relative to the bulk value and corrected for final state charging (right axis – inverted scale).

***Characterizing adsorbate binding energies and sites*:** To help elucidate the mechanism leading to the anti-correlation between BEs and activity, it is useful to understand how the reactants bind to the surface. Fig. 5 shows TPD of CO from Pd_n/TiO_2 (*J. Chem. Phys. 136, 204705 (2012)*). The feature below 180 K is assigned to a small amount of CO desorbing from TiO_2 defect sites. The two higher temperature features are seen only when Pd_n are present, and therefore represent CO desorbing from two Pd-associated sites with quite different desorption energies (E_{des}). The solid lines are simulations to the spectra, from which we can say that the ~220 K feature has E_{des} in the range from 0.5 to 0.8 eV, while the ~430 K feature has E_{des} from ~1.1 to 1.4 eV. The paper also reported TD-ISS studies which revealed that CO desorbing from sites on top of the clusters is responsible for the higher binding energies, while low binding energies are associated with CO desorbing from sites around the cluster periphery. The combination of TPD and ISS allows us to determine the energetics and qualitative nature of the binding sites, but cannot determine the binding geometry in detail. Fortunately, Liu (BNL chemistry) carried out a high level DFT study of CO binding to Pd_n/TiO_2.[15] Among other results, she found that CO binds most strongly in bridging sites on top of the clusters, but that there are sites with about half the adsorption energy at the cluster periphery, in beautiful agreement with the TD-ISS observations.

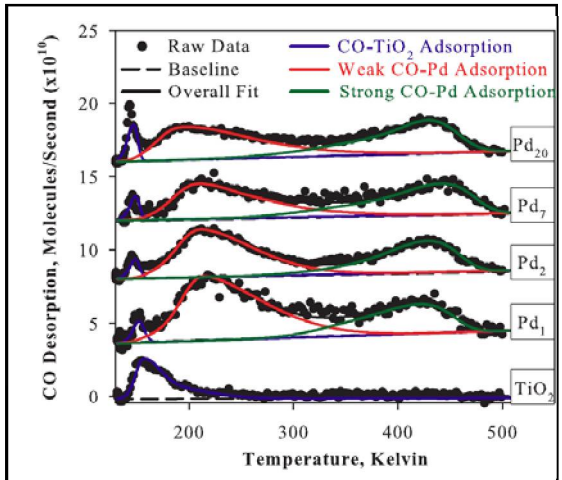

Fig. 5. CO TPD for samples with various Pd_n deposited on TiO_2, dosed at 180 K with 5 L ^{13}CO, and heated at 3 K/sec

Valence spectroscopy: We also studied the effects of cluster size and CO and O_2 binding, on the valence structure of Pd_n/TiO_2. Typical raw data near the Fermi level (E_F) is shown in Fig. 6, for TiO_2, Pd_7/TiO_2, and CO-saturated Pd_7/TiO_2. Note the presence of a small peak just below E_F for TiO_2, due to the presence of oxygen vacancies and other defect states. The sharp rise below 3 eV is the onset of the O 2p band of the TiO_2. In the energy range between E_F and the O 2p band, DOS associated with the Pd clusters can be seen, and the onset energy is size dependent, shifting closer to E_F with increasing size, to ~0.05 eV below E_F for Pd_{25}. There are also significant

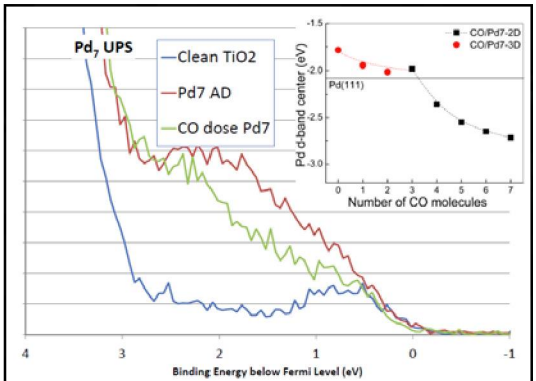

Fig. 6. Main: Near-E_F spectrum of TiO_2, Pd_7/TiO_2, and Pd_7/TiO_2 after saturation CO exposure. Inset: Results of Liu, showing that the Pd 4d band center drops upon adsorption of the last few CO molecules.

shifts from adsorption of CO and O_2.

Liu's results (inset) suggested an explanation for the effect of CO adsorption, but O_2 adsorption had an unexpectedly small effect on the near-E_F DOS. We collaborated with Shiv Khanna's group on a joint paper that developed new computational methods to distinguish the effects of orbital hybridization, cluster-support electron transfer, and photoemission final state, on the measured binding energies for both valence and core levels (*J. Phys. Chem. C,119 (2015) 6033-6046*). A second joint paper discussing adsorbate effects on binding energies is under revision for J. Phys. Chem. C. Theory is helpful in understanding details of the experiments, and in addition to the work by the Liu[15] and Khanna groups,[16-20] we have benefited from theoretical studies from the groups of Alexandrova,[21-23] and Hammer.[24] Providing data that is amenable to theoretical treatment is one motivation for this kind of work.

Additional reactivity – property correlation studies: To assess support effects on the chemistry, and on the relation between binding energies and activity, we also examined reactions catalyzed by Pd_n/alumina, using thin alumina films grown on Ta(110) and Re(0001). A study of CO oxidation over Pd_n/alumina/TiO_2(110) was published as *Faraday Discuss., 162 (2013) 323–340.* In that study, we characterized the effects of alumina film thickness on CO oxidation activity, and on the core levels of Pd, Ta, Al, and O, all of which shift with film thickness, up to ~4 nm, then become thickness-independent. CO oxidation activity was measured as a function of size for Pd_n on ~4.7 nm alumina films, with the result that activity was two to five times higher than for Pd_n/TiO_2 under the same conditions. We also reported (special issue of *Int. J. Mass Spectrom. 377 (2014) 263–277*) an analogous study of Pd_n deposited on alumina grown on Re (0001), at high temperatures, which resulted in a well ordered film,[25, 26] but also in ~2% Re incorporation into the film, as seen by ISS Re-doping of the alumina. CO oxidation activity for these systems is also anticorrelated with Pd electronic binding energies, and in addition, activity for Pd_n/alumina was found to be highly stable in repeated experiments (unlike Pd/TiO_2). It is known that dopant atoms in films can help anchor clusters with respect to diffusion,[27] and that appears to be the case here. UPS was also used to measure size-dependent shifts in the valence (i.e., Pd 4d) band, which also are anti-correlated with the activity.

2. Size-Selected Electrochemistry:

The effort in recent years focused on size-selected electrochemistry, so our DOE-supported results in this area are reviewed in somewhat more detail.

a. Pt_n/glassy carbon in acidic electrolyte: *(J. Am. Chem. Soc. 135 (2013) 3073−3086).* The goal was to study size effects on the oxygen reduction reaction (ORR) catalyzed by Pt_n on glassy carbon electrodes (GCEs), however, we also found something more interesting. We used glassy carbon because it is a commonly used electrode material that is inert at low potentials under ORR conditions. The experiments were done using the *in situ* method described above. All samples had Pt_n deposited in a 2 mm diameter spot, with loading equivalent to ~9.5% of a Pt monolayer. After completion of electrochemical experiments, the samples were removed for optical microscopy.

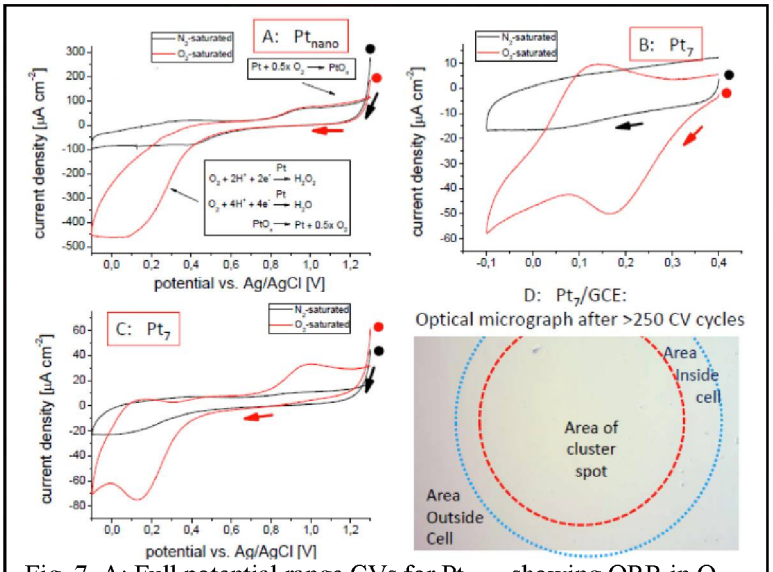

Fig. 7. A: Full potential range CVs for Pt_{nano}, showing ORR in O_2-saturated $HClO_4$ in the range between 0.3 and -0.1 V. B: CV over size selected Pt_7/GCE, showing structured ORR signal. C: Full range CV for Pt_7/GCE showing ORR at low potential and Pt oxidation at ~1 V. D: Micrograph of the electrode post reaction, with 2 mm cluster spot and 3 mm cell internal diameter indicated

Fig. 7 compares CVs for Pt_7/GCE to those measured for a GCE with 5 to 10 nm Pt particles prepared by solution deposition and annealing in H_2 ("Pt_{nano}"). The CVs were run in both N_2-purged (black) and O_2-

saturated (red) 0.1 M $HClO_4$ solutions, and potentials are given with respect to Ag/AgCl. For O_2-saturated $HClO_4$, the Pt_{nano} CV (Frame A) is dominated by strong ORR signal between -0.1 and 0.3 V. In both O_2- and N_2-purged cases, the Pt_{nano} sample shows the expected Pt redox (~0.9 V) and hydride adsorption and desorption peaks (-0.1 to 0.2 V), although they are hard to see because the ORR peak is so much larger.

For the Pt_7/GCE sample, we first examined CVs in a narrow potential range (frame B), avoiding scanning through the Pt redox potential, and then CVs over the full range (Frame C). ORR at the Pt_7 clusters is clearly seen, qualitatively similar to that seen for Pt_{nano}. The Pt_7 CVs do show some resolved structure, which is presumably washed out in the Pt_{nano} results because of the particle size distribution. The CVs were unchanged over 40 repetitions in both O_2- and N_2-saturated $HClO_4$. The peak ORR current density is ~-75 $\mu A/cm^2$, which is ~6 times lower than that observed for Pt_{nano}, which is unsurprising given that the Pt loading in the Pt_7 sample was ~10 times lower. Finally, frame D shows a post-reaction micrograph taken in near-specular illumination, with the 2mm cluster spot and the ~3 mm electrolyte-exposed area indicated. There was no visible damage.

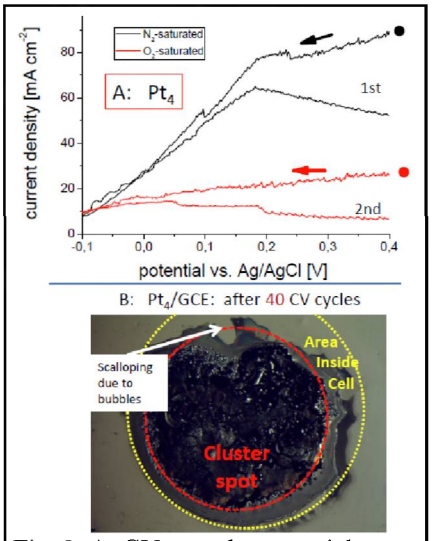

Fig. 8. A: CV over the potential range where ORR is expected, for Pt_4/GCE. B. Micrograph of Pt_4/GCE after reaction.

In contrast, many of the small clusters behave very differently, as exemplified by data for Pt_4/GCE in Fig. 8. The potential range is the same as in frame B of Fig. 7, but it can be seen that the current is positive, ~1000 times larger than seen for Pt_7, and also rather noisy and decaying with time during the scans. The "noise" is the effect of bubbles forming on the small electrodes, and the decay also results from gas displacing electrolyte. Clearly, instead of ORR, some very efficient oxidation reaction occurred, generating copious gas. The bottom of Fig. 8 shows that this reaction badly damaged the electrode, but only in the 2 mm central region where the Pt clusters were deposited. The total reaction time for this electrode was ~50 times shorter than that for the Pt_7/GCE shown in Fig. 7, i.e., the damage rate was high, and consistent with the high currents observed for Pt_4/GCE. Similar effects were observed in experiments in 0.1 M H_2SO_4. The conclusion is that the GCE was oxidized by water, catalyzed by Pt_n (reaction written in standard reduction form):

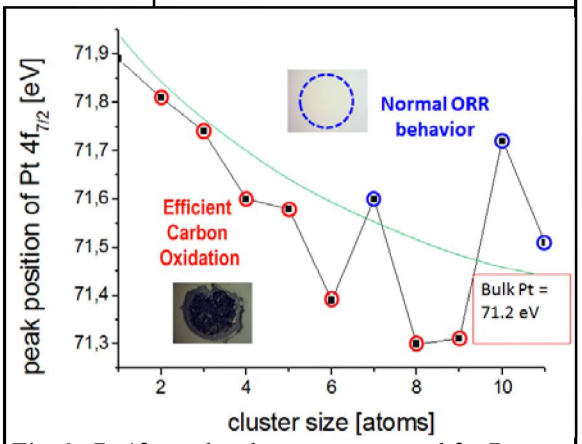

Fig. 9. Pt 4f core level energy measured for Pt_n, as deposited on GCEs, prior to electrochemical study. Also shown are post-reaction micrographs of the electrodes.

$CO_2 + 4\ H^+ + 4\ e^- \leftrightarrow C + 2\ H_2O$ $\quad E^0 = 0.01$ V vs. Ag/AgCl $\quad$ and/or

$CO + 2\ H^+ + 2\ e^- \leftrightarrow C + H_2O$ $\quad E^0 = 0.32$ V vs. Ag/AgCl

This "carbon corrosion" reaction is observed for many carbon electrodes, and is a significant degradation mechanism, but normally is rapid only at high overpotentials. Our results show that small Pt_n catalyze carbon oxidation with essentially no overpotential, raising the possibility that even small concentrations of such clusters might contribute to electrode degradation.

Fig. 9 shows one of the most interesting results of this study. This plots the energy of the Pt $4f_{7/2}$ core level as a function of cluster size, measured prior to electrochemistry. It can be seen that the values generally decrease with size, converging towards the bulk value (71.2eV), as expected from final state screening/charging considerations. Superimposed on the overall trend are oscillations, which indicate that there are considerable size-to-size variations in the electronic properties of the clusters. The oscillations are clearly related to the activity of the Pt_n/GCE for carbon oxidation, i.e., Pt_n with higher-than-trend BEs, (Pt_7, Pt_{10}, Pt_{11}) *do not* efficiently catalyze carbon oxidation by water, while the rest of the small Pt_n do.

This is a dramatic example of an anti-correlation between core level BE and activity *as an oxidation catalyst*. Here, the effects of cluster size on carbon electro-oxidation are visible with the naked eye! (Factor of >1000 variation in carbon oxidation activity).

b. Ethanol oxidation at Pt_n/ITO, n ≤ 14. (*Phys. Chem. Chem. Phys. 17 (2015) 17601-17610*). The ethanol oxidation reaction (EOR) has been studied extensively due to interest in developing direct alcohol fuel cells.[28-39] Platinum or its alloys are commonly used catalysts, because they can activate the CC bond to reach the energetically favorable CO_2 product, albeit not very efficiently. EOR is a complex reaction involving formation and reaction of multiple intermediates and products which compete for binding sites. EOR efficiency is influenced by the electronic and geometric properties of the surface, and can by modulated by alloying with Ru, Sn and other metals,[30, 40, 41] or by using different crystal planes of Pt.[28, 29, 34]

We studied the EOR under conditions similar to those used in the ORR study discussed above, i.e., N_2-purged 0.1 M $HClO_4$, but with 1 vol % of ethanol added. To avoid competition from carbon oxidation, we did these experiments using ITO thin film electrodes. Fig. 10 shows CVs for Pt_n/ITO, n ≤ 10. Note that for this and other electrochemical results below, the potentials have been converted to V vs. NHE (normal hydrogen electrode), which simply shifts the scale by 0.281 V compared to V vs. Ag/AgCl.

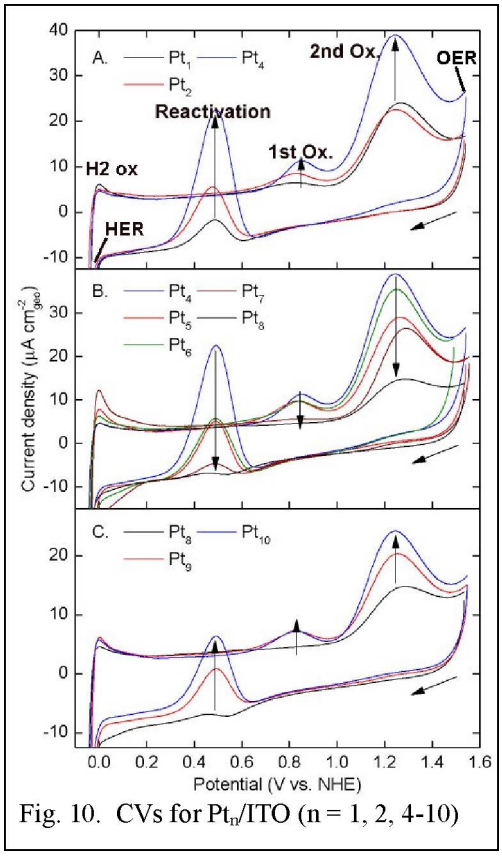

Fig. 10. CVs for Pt_n/ITO (n = 1, 2, 4-10)

Three EOR peaks are clearly seen. On the positive-going sweep there are peaks at ~0.85 V and ~1.25 V, which we will refer to as the 1st and 2nd oxidation peaks. On the negative-going sweep, a "reactivation" peak appears at ~0.48 V. In addition to these EOR peaks, the onset of the hydrogen evolution reaction (HER) and a peak for H_2 oxidation are observed near 0 V, and the onset of the oxygen evolution reaction (OER) is seen at ~1.5 V. The features are similar to what is seen for polycrystalline Pt (Pt_{poly}) or for Pt_{nano}/ITO and to results in the literature,[29-34] where vibrational spectroscopy, mass spectrometry and chromatography have been used to identify the reactions responsible. Our unique contribution is the ability to vary the cluster size.

All three EOR peaks increase substantially as size increases from Pt_1 to Pt_4, then decrease almost back to zero as size increases to Pt_8. The activity increases again to Pt_{10}, and then there is a small decrease as the size increases to Pt_{14}. Fig. 11 summarizes the EOR peak currents, normalized to the mass of Pt (1.46 x 10^{-9} g), which is precisely known in our experiments. All three peaks show similar oscillations with cluster size, consistent with the raw CVs in Fig. 10. The figure also plots the Pt $4d_{3/2}$ binding energies (BEs) measured for each sample after deposition. The BEs show large oscillations with cluster size, which are, again, strongly anti-correlated with the activities (note inverted scale).

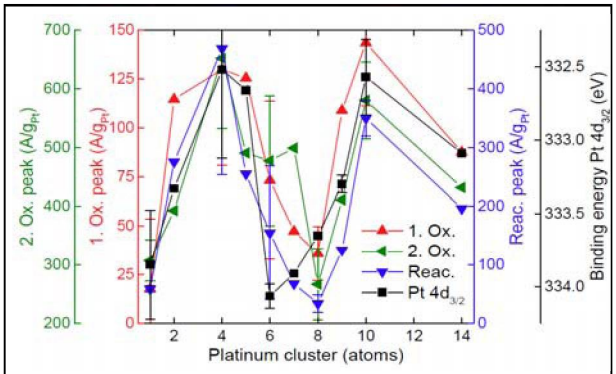

Fig. 11. Cluster size dependence of the background-subtracted peak EOR currents per gram Pt. Red: 1st oxidation peak, Green:2nd oxidation peak, Blue: reactivation peak. Black: the Pt $4d_{3/2}$ BE

There are several points to note:

1. EOR activity is sharply, and non-monotonically dependent on cluster size, and the sharp size dependence persists for at least 25 cycles through the Pt redox potential. Clearly, processes like sintering or dissolution are slow enough that the

initial size selection is preserved on this time scale.
2. EOR, HER, OER, and H_2 oxidation are observed even for the smallest cluster sizes.
3. The non-monotonic dependence on size suggests that some factor, other than simply the size of the binding sites available, is responsible for controlling EOR activity. The fact that the Pt BE is anticorrelated with activity shows that the controlling factor is Pt electronic structure.
4. While the current densities are strongly dependent on cluster size, there is little effect of size on the peak potentials, other than a slight anti-correlation between activity and the potential of the 2nd oxidation peak.

We also examined the coverage dependence of EOR for Pt_1, because there is evidence from STM,[42, 43] ion scattering,[3, 10, 44, 45] and reactivity studies,[5] that that noble metal atoms on oxides are more prone to sintering, compared to pre-formed, deposited clusters. Indeed, there is some evidence that Pt_1 sinters at higher coverages to make small clusters, although it appears that the number of clusters present is still small, i.e., even atoms remain largely un-sintered. Changes observed in EOR currents over time, during ~100 CV cycles, are discussed below.

c. ORR at Pt_n/ITO, n ≤ 14. (*J. Phys. Chem. C, 119 (2015) 11160–11170)* This work was published in a special issue reporting highlights of the 2014 ISSPIC meeting in Japan. Briefly, ORR was studied under conditions identical to those used in the Pt_n/glassy carbon work mentioned above, but with inert ITO substrates. Fig. 12 compares typical CVs for Pt_5/ITO to those measured for Pt_{nano}/ITO (i.e., 5-10 nm Pt particles on ITO). (Small ORR currents are observed in the N_2-purged CVs because the O_2-saturated CVs were done first, and it is difficult to flush out all the electrolyte *in situ*). The ORR current density *per* gram Pt is ~10 times higher for Pt_5 than Pt_{nano}, but this expected because the clusters have all the Pt in the surface layer.

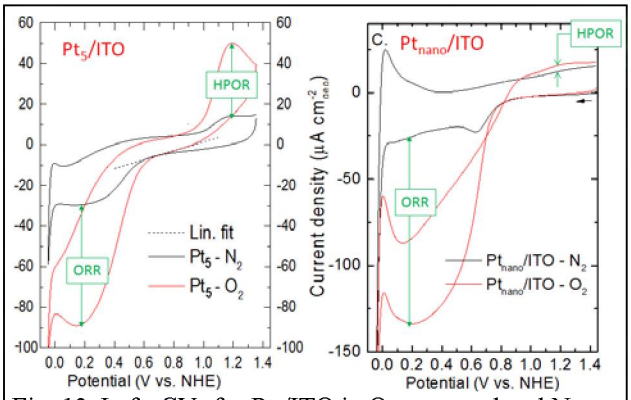

Fig. 12. Left: CVs for Pt_5/ITO in O_2 saturated and N_2-purged $HClO_4$. Right: CVs for an ITO substrate with 1 ML Pt in the form of 5-10 nm Pt particles.

The more interesting observation is that for the small clusters, there are substantial peaks at high potential due to the hydrogen peroxide oxidation reaction (HPOR). This tells us something interesting about the product branching in ORR. The two reactions possible in ORR are:

$$O_2 + 4\ e^- + 4\ H^+ \rightarrow 2\ H_2O \qquad \text{and} \qquad O_2 + 2\ e^- + 2\ H^+ \rightarrow H_2O_2.$$

As discussed by Katsounaros *et al.*,[46] H_2O_2 that is formed during ORR at low potentials is oxidized back to O_2 at high potentials, catalyzed by the oxidized Pt surface that forms above ~0.8 V. The much larger HPOR/ORR current ratio for Pt_5/ITO, compared to Pt_{nano}/ITO, indicates that the small clusters have a large branching ratio for H_2O_2 formation during ORR. Fig. 13 shows how the HPOR/ORR ratio varies with size. The point at the far right is for Pt_{nano}/ITO, and the ratio for polycrystalline Pt is similar. Note that the HPOR/ORR ratio is over 50% for Pt_1, dropping to ~25% for Pt_{14}, and ~3% for Pt_{nano}. The trend is what might be expected if the physical size of the available binding sites controls the branching. For large clusters or nanoparticles, O_2 dissociation leads to formation of 2 H_2O, but atoms or very small clusters may not have sites able to dissociate O_2, thus leading to H_2O_2. The inability to dissociate O_2 could be a purely geometric effect, especially for the smallest clusters, however, the XPS results in Fig.11 show that the electronic properties of the Pt_n/ITO vary strongly with size, thus electronic effects may also be important.

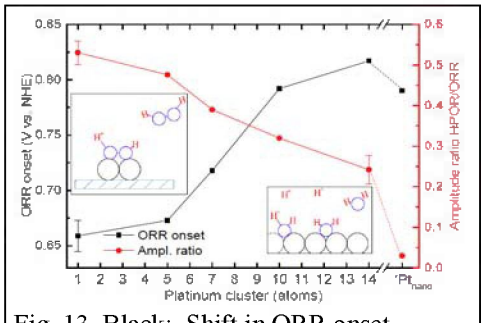

Fig. 13. Black: Shift in ORR onset potential with Pt_n size. Red: HPOR/ORR ratio as a function of size.

As shown above, for both UHV CO oxidation, and for EOR and carbon electro-oxidation, the metal core level BEs were anti-correlated with activity. As discussed in our paper,[14] both initial and final state perspectives suggest that low BEs

reflect electron-rich metal centers, while high BEs indicate electron-poor clusters. The anti-correlation, therefore, provides the insight that high activity for oxidation catalysis is associated with electron-rich metal centers. This may seem counterintuitive for oxidation, however, the rate-limiting step is not the actual oxidation event, but rather activation of O_2, CH and OH bonds in the reactants,[39] which may be driven by electron donation to antibonding orbitals.

IV. Summary

This grant enabled a number studies of the effects of cluster size on catalytic activity under both UHV surface science and aqueous electrochemistry conditions. In nearly all systems examined, substantial effects of cluster size on activity were observed, and by carrying out spectroscopic and other surface science experiments on the models catalysts, it was possible to identify the factor(s) responsible for the cluster size effects, i.e., the factors that control the rate-limiting step.

V. List of publications acknowledging support from this grant

1. "Sintering, Oxidation, and Chemical Properties of Size-Selected Nickel Clusters on TiO_2 (110)", by Masato Aizawa, Sungsik Lee, and Scott L. Anderson., J. Chem. Phys. **117** (2002) 5001-11, DOI: 10.1063/1.1498477
2. "Deposition dynamics and chemical properties of size-selected Ir clusters on TiO_2", Masato Aizawa, Sungsik Lee, and Scott L. Anderson, Surf. Sci. 542 (2003) 253-75, DOI: 10.1016/S0039-6028(03)00984-1
3. "CO oxidation on Au_n/TiO_2 catalysts produced by size-selected cluster deposition" Sungsik Lee, Chaoyang Fan, Tianpin Wu, and Scott L. Anderson, JACS (comm) 126 (2004) 5682-3, DOI: 10.1021/ja049436v
4. "Cluster size effects on CO oxidation activity, adsorbate affinity, and temporal behavior of model Au_n/TiO_2 catalysts", Sungsik Lee, Chaoyang Fan, Tianpin Wu, and Scott L. Anderson, J. Chem. Phys. 123 (2005) 124710/1 – 124710/13, DOI: 10.1063/1.2035098.
5. "Agglomeration, Support Effects, and CO Adsorption on Au/TiO_2 (110) Prepared by Ion Beam Deposition" Sungsik Lee, Chaoyang Fan, Tianpin Wu, and Scott L. Anderson, Surf. Sci. 578 (2005) 5-19, DOI: 10.1016/j.susc.2005.01.017
6. "Agglomeration, Sputtering, and Carbon Monoxide Adsorption Behavior for Au/Al_2O_3 Prepared by Au_n^+ Deposition on Al_2O_3/NiAl(110)", Sungsik Lee, Chaoyang Fan, Tianpin Wu, and Scott L. Anderson, J. Phys. Chem. B 109 (2005) 11340-11347, DOI: 10.1021/jp0502407
7. "Water on rutile TiO_2(110) and Au/TiO_2(110): Effects on Au mobility and the isotope exchange reaction", Tianpin Wu, William E. Kaden and Scott L. Anderson, J. Phys. Chem. C.; 112; (2008), 9006-9015. DOI: 10.1021/jp800521q
8. "Size-dependent oxidation of Pd_n ($n \leq 13$) on alumina/NiAl(110): Correlation with Pd core level binding energies." Tianpin Wu, William E. Kaden, William A. Kunkel, and Scott L. Anderson, Surf. Sci. 603 (2009) 2764-77, doi:10.1016/j.susc.2009.07.014.
9. "Electronic Structure Controls Reactivity of Size-Selected Pd Clusters Adsorbed on TiO_2 Surfaces", William E. Kaden, Tianpin Wu, William A. Kunkel, Scott L. Anderson, Science. 326 (2009) 826 - 9. DOI: 10.1126/science.1180297
10. "CO Adsorption and Desorption on Size-Selected Pd_n/TiO_2 Model Catalysts: Size Dependence of Binding Sites and Energies, and Support-Mediated Adsorption" William E. Kaden, William A. Kunkel, F. Sloan Roberts, Matthew Kane and Scott L. Anderson, J. Chem. Phys. 136 (2012) 204705 12 pages, doi: 10.1063/1.4721625
11. "Strong effects of cluster size and air exposure on oxygen reduction and carbon oxidation electrocatalysis by size-selected Ptn ($n \leq 11$) on glassy carbon electrodes", Sebastian Proch, Mark Wirth, Henry S. White, and Scott L. Anderson, J. Am. Chem. Soc. **135** (2013) 3073−3086, DOI: 10.1021/ja309868z
12. "Alumina support and Pd_n cluster size effects on activity of Pd_n for catalytic oxidation of CO", Matthew D. Kane, R. Sloan Roberts, and Scott L. Anderson, Faraday Disc., 162 (2013) 323 - 340, DOI: 10.1039/c3fd20151a

13. "Hollow cathode lamp with integral, high optical efficiency isolation valve: A modular VUV source", F. Sloan Roberts and Scott L. Anderson, Rev. Sci. Instrum. 84, (2013) 126101 (3 pages); doi: 10.1063/1.4838675
14. "Mass-selected supported cluster catalysts: Size effects on CO oxidation activity, electronic structure, and thermal stability of Pd_n/alumina ($n \leq 30$) model catalysts" Matthew D. Kane, F. Sloan Roberts, and Scott L. Anderson, Int. J. Mass Spectrom. 370 (2014) 1-15, DOI: 10.1016/j.ijms.2014.06.018, and Special Issue "MS 1960 to Now" 10.1016/j.ijms.2014.07.044
15. "Cluster Size Controls Branching Between Water And Hydrogen Peroxide Production In Electrochemical Oxygen Reduction at Pt_n/ITO" Alexander von Weber, Eric T. Baxter, Henry S. White, and Scott L. Anderson, J. Phys. Chem. C 119 (2015) 11160–11170, DOI: 10.1021/jp5119234
16. "Initial and Final State Effects in the Ultraviolet and X-Ray Photoelectron Spectroscopy (UPS and XPS) of Size-Selected Pd_n clusters Supported on TiO2(110)", F. Sloan Roberts, Scott L. Anderson, Arthur C. Reber, and Shiv N. Khanna, J. Phys. Chem. C 119 (2015) 6033-6046. DOI: 10.1021/jp512263w
17. "Size-Dependent Electronic Structure Controls Activity for Ethanol Electro-Oxidation at Pt_n/Indium Tin Oxide (n = 1 to 14)", Alexander von Weber, Eric T. Baxter, Sebastian Proch, Matthew D. Kane, Michael Rosenfelder, Henry S. White, and Scott L. Anderson, Phys.Chem.Chem.Phys. 17 (2015) 17601-17610, DOI: 10.1039/C5CP01824B
18. "The Effect of O_2 and CO Exposure on the Photoelectron Spectroscopy of Size-selected Pd_n Clusters Supported on TiO_2(110)", Arthur C. Reber, Shiv N. Khanna, F. Sloan Roberts, Scott L. Anderson. J. Phys. Chem. C (in revision 10/2015)

Bibliography and References Cited.

1. W. E. Kaden, W. A. Kunkel, F. S. Roberts, M. Kane, and S. L. Anderson, *CO adsorption and desorption on size-selected Pdn/TiO2(110) model catalysts: Size dependence of binding sites and energies, and support-mediated adsorption.* J. Chem. Phys., 2012. **136**: p. 204705/1-204705/12.
2. W. E. Kaden, W. A. Kunkel, M. D. Kane, F. S. Roberts, and S. L. Anderson, *Size-Dependent Oxygen Activation Efficiency over Pdn/TiO2(110) for the CO Oxidation Reaction.* J. Am. Chem. Soc., 2010. **132**: p. 13097–13099.
3. W. E. Kaden, W. A. Kunkel, and S. L. Anderson, *Cluster size effects on sintering, CO adsorption, and implantation in Ir/SiO_2.* J. Chem. Phys., 2009. **131**: p. 114701, 1-15.
4. S. Proch, M. Wirth, H. S. White, and S. L. Anderson, *Strong Effects of Cluster Size and Air Exposure on Oxygen Reduction and Carbon Oxidation Electrocatalysis by Size-Selected Pt_n ($n \leq 11$) on Glassy Carbon Electrodes.* J. Am. Chem. Soc., 2013. **135**: p. 3073−3086.
5. F. S. Roberts, M. D. Kane, E. T. Baxter, and S. L. Anderson, *Oxygen activation and CO oxidation over size-selected Ptn/alumina/Re(0001) model catalysts: correlations with valence electronic structure, physical structure, and binding sites.* Phys. Chem. Chem. Phys., 2014. **16**: p. 26443 – 26457.
6. M. D. Kane, F. S. Roberts, and S. L. Anderson, *Effects of Alumina Thickness on CO Oxidation Activity over Pd_{20}/Alumina/Re(0001): Correlated Effects of Alumina Electronic Properties and Pd_{20} Geometry on Activity.* J. Phys. Chem. C, 2015. **119**: p. 1359–1375.
7. M. D. Kane, F. S. Roberts, and S. L. Anderson, *Alumina support and Pd_n cluster size effects on activity of Pd_n for catalytic oxidation of CO.* Faraday Disc., 2013. **162**: p. 323 - 340.
8. M. Aizawa, S. Lee, and S. L. Anderson, *Sintering, Oxidation, and Chemical Properties of Size-Selected Nickel Clusters on TiO2 (110).* J. Chem. Phys., 2002. **117**: p. 5001-5011.
9. M. Aizawa, S. Lee, and S. L. Anderson, *Deposition dynamics and chemical properties of size-selected Ir clusters on TiO2.* Surf. Sci., 2003. **542**: p. 253-275.
10. S. Lee, C. Fan, T. Wu, and S. L. Anderson, *Cluster size effects on CO oxidation activity, adsorbate affinity, and temporal behavior of model Aun/TiO2 catalysts.* J. Chem. Phys., 2005. **123**: p. 124710/1 – 124710/13.

11. C. Fan, T. Wu, W. E. Kaden, and S. L. Anderson, *Cluster size effects on hydrazine decomposition on Irn/Al2O3/NiAl(110).* Surf. Sci., 2006. **600**: p. 461-7.
12. M. D. Kane, F. S. Roberts, and S. L. Anderson, *Mass-selected supported cluster catalysts: Size effects on CO oxidation activity, electronic structure, and thermal stability of Pd_n/alumina ($n \leq 30$) model catalysts.* Int. J. Mass Spectrom., 2014. **370**: p. 1-15.
13. A. von Weber, E. T. Baxter, H. S. White, and S. L. Anderson, *Cluster Size Controls Branching Between Water And Hydrogen Peroxide Production In Electrochemical Oxygen Reduction at Pt_n/ITO.* J. Phys. Chem. C, 2015. **119**: p. 11160–11170.
14. A. von Weber, E. T. Baxter, S. Proch, M. D. Kane, M. Rosenfelder, H. S. White, and S. L. Anderson, *Size-Dependent Electronic Structure Controls Activity for Ethanol Electro-Oxidation at Pt_n/Indium Tin Oxide (n = 1 to 14).* Phys Chem Chem Phys, 2015. **17**: p. 17601-17610.
15. P. Liu, *Understanding the Behavior of TiO_2(110)-Supported Pd_7 Cluster: A Density Functional Study.* J. Phys. Chem. C 2012. **116**: p. 25337−25343.
16. S. V. Ong and S. N. Khanna, *Theoretical Studies of the Stability and Oxidation of Pdn (n = 1-7) Clusters on Rutile TiO2(110): Adsorption on the Stoichiometric Surface.* J. Phys. Chem. C, 2012. **116**: p. 3105-3111.
17. S. V. Ong and S. N. Khanna, *Enhanced oxygen binding through surface mediated ionic bonds.* Surf. Sci., 2012. **606**: p. 965-970.
18. S. V. Ong and S. N. Khanna, *Origin of Oxidation and Support-Induced Structural Changes in Pd4 Clusters Supported on TiO2.* J. Phys. Chem. C, 2011. **115**: p. 20217-20224.
19. R. Robles and S. N. Khanna, *Oxidation of Pdn (n=1-7, 10) clusters supported on alumina/NiAl(110).* Phys. Rev. B: Condens. Matter Mater. Phys., 2010. **82**: p. 085428/1-085428/6.
20. A. C. Reber and S. N. Khanna, *Effect of N- and P-Type Doping on the Oxygen-Binding Energy and Oxygen Spillover of Supported Palladium Clusters.* J. Phys. Chem. C, 2014. **118**: p. 20306–20313.
21. J. Zhang and A. N. Alexandrova, *Structure, stability, and mobility of small Pd clusters on the stoichiometric and defective TiO2 (110) surfaces.* J. Chem. Phys., 2011. **135**: p. 174702/1-174702/10.
22. J. Zhang and A. N. Alexandrova, *Aromaticity in a surface deposited cluster: Pd4 on TiO2 (110).* arXiv.org, e-Print Arch., Condens. Matter, 2011: p. 1-4, arXiv:1112 4032v1 [cond-mat mtrl-sci].
23. J. Dadras, E. Jimenez-Izal, and A. N. Alexandrova, *Alloying Pt Sub-nano-clusters with Boron: Sintering Preventative and Coke Antagonist?* ACS Catalysis, 2015: p. 5719-5727.
24. J. G. Wang and B. Hammer, *Role of Au+ in supporting and activating Au7 on TiO2(110).* Phys. Rev. Lett., 2006. **97**: p. 136107.
25. X. Lai, C. C. Chusuei, K. Luo, Q. Guo, and D. W. Goodman, *Imaging ultrathin Al2O3 films with scanning tunneling microscopy.* Chem. Phys. Lett., 2000. **330**: p. 226-230.
26. Y. Wu, E. Garfunkel, and T. E. Madey, *Growth and oxidation of ultra-thin Al films on the Re(0001) surface.* Surf. Sci., 1996. **365**: p. 337-352.
27. Y. Cui, K. Huang, N. Nilius, and H.-J. Freund, *Charge competition with oxygen molecules determines growth of gold nanoparticles on CaO films.* Faraday Disc., 2013. **162**: p. 153-163.
28. S. C. S. Lai and M. T. M. Koper, *Electro-oxidation of ethanol and acetaldehyde on platinum single-crystal electrodes.* Faraday Discuss., 2008. **140**: p. 399-416.
29. F. Colmati, G. Tremiliosi-Filho, E. R. Gonzalex, A. Berna, E. Herrero, and J. M. Feliu, *Surface structure effects on the electrochemical oxidation of ethanol on platinum single crystal electrodes.* Faraday Discuss., 2008. **140**: p. 379-397.
30. F. Vigler, C. Coutanceau, F. Hahn, E. M. Belgsir, and C. Lamy, *On the mechanism of ethanol electo-oxidation on Pt and PtSn catalysts: electrochemical and in situ IR reflectance spectroscopy studies.* J. Electroanal. Chem., 2004. **563**: p. 81-89.
31. R. A. Rightmire, R. L. Rowland, D. L. Boos, and D. L. Beal, *Ethyl Alcohol Oxidation at Platinum Electrodes.* J. Electrochem. Soc., 1964. **111**: p. 242-247.

32. L.-W. H. Leung, S.-C. Chang, and M. J. Weaver, *Real-time FTIR spectroscopy as an electrochemical mechanistic probe. Electrooxidation of ethanol and related species on well-defined Pt(111) surfaces.* J. Electroanal. Chem., 1989. **266**: p. 317-336.
33. H. Wang, Z. Jusys, and R. J. Behm, *Ethanol Electrooxidation on a Carbon Supported Pt Catalyst: Reaction Kinetics and Product Yields.* J. Phys. Chem. B, 2004. **108**: p. 19413-19424.
34. M. J. Giz and G. A. Camara, *The ethanol electrooxidation reaction at Pt (111): The effect of ethanol concentration.* J. Electroanal. Chem., 2009. **652**: p. 117-122.
35. I. G. Casella and E. Desimoni, *XPS, SEM and Electrochemical Characterization of a Platinum-Based Glassy Carbon Modified Electrode: Electrocatalytic Oxidation of Ethanol in Acidic Medium.* Electroanalysis, 1996. **8**: p. 447-453.
36. J. F. Gomes, K. Bergamaski, M. F. S. Pinto, and P. B. Miranda, *Reaction intermediates of ethanol electro-oxidation on platinum investigated by SFG spectroscopy.* J. Catal., 2013. **302**: p. 67-82.
37. F. Vigier, C. Coutanceau, A. Perrard, E. M. Belgsir, and C. Lamy, *Development of anode catalysts for a direct ethanol fuel cell.* J. Appl. Electrochem. , 2004. **34**: p. 439–446.
38. A. Kowal, M. Li, M. Shao, K. Sasaki, M. B.Vukmirovic, J. Zhang, N. S. Marinkovic, P. Liu, A. Frenkel, and R. R. Adzic, *Ternary Pt/Rh/SnO2 Electrocatalysts for Oxidizing Ethanol to CO2.* Nat. Mater., 2009. **8**: p. 325-330.
39. M. Neurock, *First-principles modeling for the electro-oxidation of small molecules*, in *Handbook of Fuel Cells – Fundamentals, Technology and Applications, Vol. 5 Advances in Electocatalysis, Materials, Diagnostics and Durability*, Wolf Vielstich, Harumi Yokokawa, and Hubert A. Gasteiger, Editors. 2009, John Wiley& Sons, Ltd.: London
40. S. St. John, P. Boolchand, and A. P. Angelopoulos, *Improved Electrocatalytic Ethanol Oxidation Activity in Acidic and Alkaline Electrolytes Using Size-Controlled Pt–Sn Nanoparticles.* Langmuir, 2013. **29**: p. 16150-16159.
41. H. Wang, Z. Jusys, and R. J. Behm, *Ethanol electrooxidation on carbon-supported Pt, PtRu and Pt3Sn catalysts - a quantitative DEMS study.* J. Power Sources, 2006. **154**: p. 351-359.
42. L. Benz, X. Tong, P. Kemper, Y. Lilach, A. Kolmakov, H. Metiu, M. T. Bowers, and S. K. Buratto, *Landing of size-selected Agn+ clusters on single crystal TiO2(110)-1x1 surfaces at room temperature.* J. Chem. Phys., 2005. **122**: p. 081102-1 - 081102-4.
43. X. Tong, L. Benz, P. Kemper, H. Metiu, M. T. Bowers, and S. K. Buratto, *Intact Size-Selected Aun Clusters on a TiO2(110)-(1 x 1) Surface at Room Temperature.* J. Am. Chem. Soc., 2005. **127**: p. 13516-18.
44. S. Lee, C. Fan, T. Wu, and S. L. Anderson, *Agglomeration, Sputtering, and Carbon Monoxide Adsorption Behavior for Au/Al2O3 Prepared by Aun+ Deposition on Al2O3/NiAl(110).* J. Phys. Chem. B, 2005. **109**: p. 11340-11347.
45. S. Lee, C. Fan, T. Wu, and S. L. Anderson, *Agglomeration, Support Effects, and CO Adsorption on Au/TiO2(110) Prepared by Ion Beam Deposition.* Surface Science, 2005. **578**: p. 5-19.
46. I. Katsounaros, W. B. Schneider, J. C. Meier, U. Benedikt, P. U. Biedermann, A. A. Auer, and K. J. J. Mayrhofer, *Hydrogen peroxide electrochemistry on platinum: towards understanding the oxygen reduction reaction mechanism.* Phys Chem Chem Phys, 2012. **14**: p. 7384-7391.